ACS OMEGA

http://pubs.acs.org/journal/acsodf

Article

Structural, Electronic, and Nonlinear Optical Properties of $C_{66}H_4$ and $C_{70}Cl_6$ Encapsulating Li and F Atoms

Ying Zhang, Zhao Zheng, Yitao Si, Baisheng Sa,* Hengyi Li, Tao Yu,* Cuilian Wen, and Bo Wu

Cite This: *ACS Omega* 2021, 6, 16234−16240

Read Online

ACCESS | Metrics & More | Article Recommendations

ABSTRACT: Recently, nonclassical fullerene derivatives $C_{66}H_4$ and $C_{70}Cl_6$, which both contain two negatively curved moieties of heptagons, have been successfully synthesized. Inspired by these experimental achievements, the structural and electronic properties of $C_{66}H_4$, $C_{70}Cl_6$, $Li@C_{66}H_4$, $F@C_{66}H_4$, $Li@C_{70}Cl_6$, and $F@C_{70}Cl_6$ were systematical studied through density functional theory calculations in this work. Our results show that the reduction of the front molecular orbital gap of fullerene derivatives occurs with the introduction of Li and F atoms. After quantitative analysis of back-donations of charge between an encapsulated atom and an external carbon cage, it is found that $C_{66}H_4$ and $C_{70}Cl_6$ prefer to act as electron acceptors. It is interesting to note that the strong covalent nature of the interactions between a F atom and a carbon cage is observed, whereas the weak covalent and strong ionic interactions occur between a Li atom and a carbon cage. On the other hand, according to the first hyperpolarizability results, the encapsulation of the Li atom enhances the nonlinear optical response of fullerene derivatives. This work provides a strategy to improve nonlinear optical properties of $C_{66}H_4$ and $C_{70}Cl_6$, reveals the internal mechanism of the contribution from Li and F atoms to endohedral fullerene derivatives, and will contribute to the designation of endohedral fullerene derivative devices.

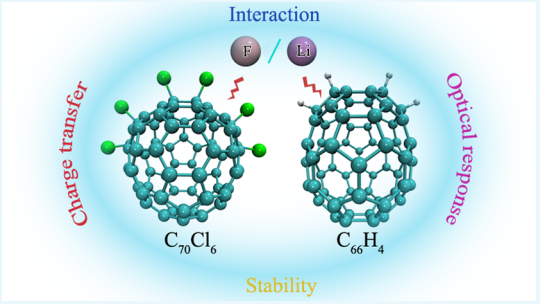

INTRODUCTION

Since the discovery of the first fullerene C_{60} by Kroto et al.[1] in the experiment of laser gasification of graphite in 1985, fullerenes have attracted extensive attention due to their unique physical and chemical properties.[2−8] Later, structural characterization confirmed that C_{60} is a closed cage structure composed of 20 hexagons and 12 nonadjacent pentagons, where the 60 carbon atoms are completely equivalent, adding a new allotrope to the elemental carbon family. Nowadays, fullerenes have been defined as closed cage-like carbon cluster molecules composed of carbon atoms, in which the carbon atoms are sp^2 hybridized and three-fold coordinated. The distinctive cavity structure of fullerenes allows them to trap atoms or clusters and form the so-called endohedral fullerenes.[9] The first macroscopic quantity of endohedral fullerene $La@C_{82}$ was synthesized by Smalley et al.[10] in 1991, and since then, a wide variety of endohedral fullerenes have been developed.[11−16] Compared with parent fullerenes, endohedral fullerenes have been found to have better performance due to the charge transfer between trapped atoms and the external carbon cage, which make them important in various fields such as organic electronics,[17] biomedicine,[18,19] cosmetics,[20] nonlinear optics,[21,22] etc.

Fullerenes following the well-known isolated-pentagon rule (IPR) only containing pentagons and hexagons are "classical fullerenes".[23] Outside of this rule, the so-called "nonclassical" fullerenes containing quadrilaterals or heptagons have been found.[24,25] Recently, researchers have synthesized two nonclassical fullerene chloride- and hydride-containing heptagons, $C_{70}Cl_6$ and $C_{66}H_4$.[26,27] In previous experiments, all of the synthesized C_{70} isomers had a positive curvature. $C_{70}Cl_6$ is the first nonclassical C_{70} fullerene derivative that possesses two negatively curved heptagons captured in situ from a chlorine-containing carbon arc. On the other hand, $C_{66}H_4$ is the first nonclassical fullerene containing two heptagons and features with its smallest size among synthesized fullerenes with two heptagons currently. Interestingly, for both $C_{70}Cl_6$ and $C_{66}H_4$, two pairs of double-fused pentagons can be observed, which are exactly fused to two concave heptagons. Theoretical calculation results discover that the strain in the fused pentagons is released by the adjacent heptagon, the modified chlorine, and hydrogen atoms. Meanwhile, the sp^2-hybridized carbon atoms connected with chlorine and hydrogen atoms are converted into sp^3-hybridized atoms.

Considering that Li and F are the elements with low first ionization energy and high electron affinity,[28] respectively, we

Received: May 5, 2021
Accepted: June 3, 2021
Published: June 14, 2021

suppose that introducing these elements into the nonclassical $C_{70}Cl_6$ and $C_{66}H_4$ will exert a distinctive influence on their electronic properties, and thus on their application performance. At present, the scale of previous studies on encapsulating Li and F atoms into fullerenes is limited, and nonetheless, their results favor that Li- and F-encapsulated endohedral fullerenes have novel properties.[29−32] It is, therefore, valuable to investigate the interactions between the internal Li and F atoms and the $C_{66}H_4$ and $C_{70}Cl_6$ carbon cages for fullerene designation and its property improvement. In this work, we have systematically studied the geometries and electronic properties of $C_{66}H_4$ and $C_{70}Cl_6$ with encapsulating Li and F atoms based on density functional theory calculations. Despite fundamental physical chemistry properties, we also focus on the influences of Li atoms on nonlinear optical properties of $C_{66}H_4$ and $C_{70}Cl_6$ that directly reflect the application value of these nonclassical endohedral fullerenes.

RESULTS AND DISCUSSION

Optimized geometries of $C_{66}H_4$, $C_{70}Cl_6$, $Li@C_{66}H_4$, $F@C_{66}H_4$, $Li@C_{70}Cl_6$, and $F@C_{70}Cl_6$ are presented in Figure 1. The

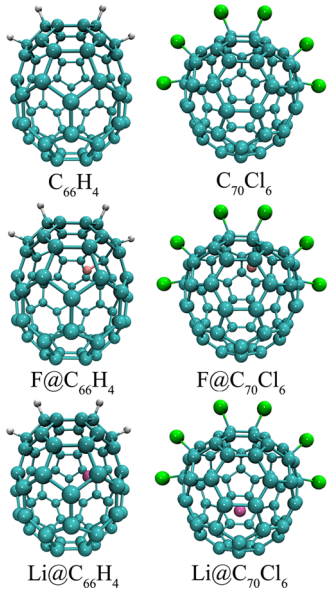

Figure 1. Optimized geometries of $C_{66}H_4$, $C_{70}Cl_6$, $F@C_{66}H_4$, $F@C_{70}Cl_6$, $Li@C_{66}H_4$, and $Li@C_{70}Cl_6$. Cyan, white, green, pink, and mauve balls denote C, H, Cl, F, and Li atoms, respectively.

detailed bond lengths, radii that coordinate the carbon cage center along *X*, *Y*, and *Z* directions, and encapsulation energies of fullerene derivatives are given in Table 1. As shown in Table 1, compared with $C_{66}H_4$ and $C_{70}Cl_6$, slightly changes in the bond lengths of C_{5-5} and C_{5-7} are observed on $Li@C_{66}H_4$, $F@C_{66}H_4$, $Li@C_{70}Cl_6$, and $F@C_{70}Cl_6$. Moreover, their radii in the *X*, *Y*, and *Z* directions are almost equal to the corresponding values in $C_{66}H_4$ and $C_{70}Cl_6$ too. Therefore, the encapsulation of F and Li atoms has a limited effect on the deformation of the total cage framework. However, it is noted that F atoms cause the collapse of the local C atoms in the carbon cage. This phenomenon is due to the strong covalent interaction between the F atom and the carbon cage. In addition, $F@C_{66}H_4$ and $F@C_{70}Cl_6$ have larger encapsulation energies (64.07 and 64.81 kcal/mol) than the Li encapsulation cases, reflecting that the

Table 1. Bond Lengths for C_{5-5} (Pentagon−Pentagon, d_{5-5}, Å) and C_{5-7} (Pentagon−Heptagon, d_{5-7}, Å), Encapsulation Energies (E_{en}, kcal/mol) of $X@C_{66}H_4$ and $X@C_{70}Cl_6$ (X = F and Li), and Their Radii along the r_X, r_Y, and r_Z (Å) Directions

molecule	d_{5-5}	d_{5-7}	E_{en}	r_X	r_Y	r_Z
$F@C_{66}H_4$	1.59−1.59	1.53−1.54	64.07	3.84	3.26	3.96
$Li@C_{66}H_4$	1.59−1.60	1.54−1.54	42.38	3.84	3.28	3.95
$F@C_{70}Cl_6$	1.61−1.62	1.52−1.53	64.81	3.49	3.74	4.78
$Li@C_{70}Cl_6$	1.62−1.62	1.52−1.52	39.53	3.48	3.74	4.77
$C_{66}H_4$	1.59	1.54		3.85	3.28	3.94
$C_{70}Cl_6$	1.62	1.52		3.46	3.75	4.80

encapsulation of F atoms in the fullerene cages is easier than that of Li atoms.

Infrared spectroscopy of endohedral fullerenes is an effective method to elucidate the cage structure.[33] In this study, infrared spectra of $X@C_{66}H_4$ and $X@C_{70}Cl_6$ (X = F and Li) are simulated and are shown in Figure 2. It can be observed that some weak absorption peaks are distributed under 200 cm^{-1}, which are caused by the vibration of Li and F atoms. The absorption peaks in 200−1000 cm^{-1} correspond to the "breathing" mode of the carbon cage, while the absorption peaks above 1000 cm^{-1} originate from the C−C stretching mode of the carbon cage. For $X@C_{66}H_4$ (X = F and Li), the absorption peak at 2900−3000 cm^{-1} corresponds to the C−H tensile vibration. In addition, the intensity of the absorption peaks of $Li@C_{66}H_4$ and $Li@C_{70}Cl_6$ is stronger than their parent cage, while the intensity of the absorption peaks of $F@C_{66}H_4$ and $F@C_{70}Cl_6$ is weaker than their parent cage. This is because the doping of Li and F atoms introduces the change of charge distribution and the dipole moment, which further results in a change in the intensity of the absorption peaks. We, thus, performed static polarizability and dipole moment calculations, and the results are given in Table 2. Compared with $F@C_{66}H_4$ and $F@C_{70}Cl_6$, $Li@C_{66}H_4$ and $Li@C_{70}Cl_6$ have higher dipole moments and polarities, so their corresponding intensities of absorption peaks are stronger.

Frontier molecular orbitals of $X@C_{66}H_4$ and $X@C_{70}Cl_6$ (X = F and Li) were calculated to analyze their electronic properties and stabilities. Figure 3 shows their highest occupied molecular orbital (HOMO), lowest unoccupied molecular orbital (LUMO), and HOMO−LUMO gap, which includes the frontier molecular orbitals of empty $C_{66}H_4$ and $C_{70}Cl_6$ for comparison. For empty $C_{66}H_4$, the HOMO level is −6.92 eV, while the LUMO level is −2.90 eV, and hence the HOMO−LUMO gap equals to 4.02 eV. For empty $C_{70}Cl_6$, the corresponding values are −7.54, −3.30, and 4.24 eV, respectively. As presented in Figure 3, compared with $C_{66}H_4$ and $C_{70}Cl_6$, the HOMO−LUMO gaps of $X@C_{66}H_4$ and $X@C_{70}Cl_6$ (X = F and Li) are all declined. This result is mainly attributed to the introduction of additional Li and F energy levels, which thereby reduce the HOMO−LUMO gap. The stability of thermally dynamically favored fullerene can also be judged with HOMO−LUMO gaps. Generally, fullerenes with a smaller HOMO−LUMO gap possess lower dynamic stability and higher reactivity.[34] According to Figure 3, the HOMO−LUMO gaps of $F@C_{66}H_4$ and $F@C_{70}Cl_6$ are larger than those of $Li@C_{66}H_4$ and $Li@C_{70}Cl_6$, indicating the better stability of fullerene derivatives encapsulating a F atom. The charge distributions are also shown in Figure 3. For $Li@C_{66}H_4$ and $Li@C_{70}Cl_6$, the electron density distribution around Li atoms

https://doi.org/10.1021/acsomega.1c02364
ACS Omega 2021, 6, 16234−16240

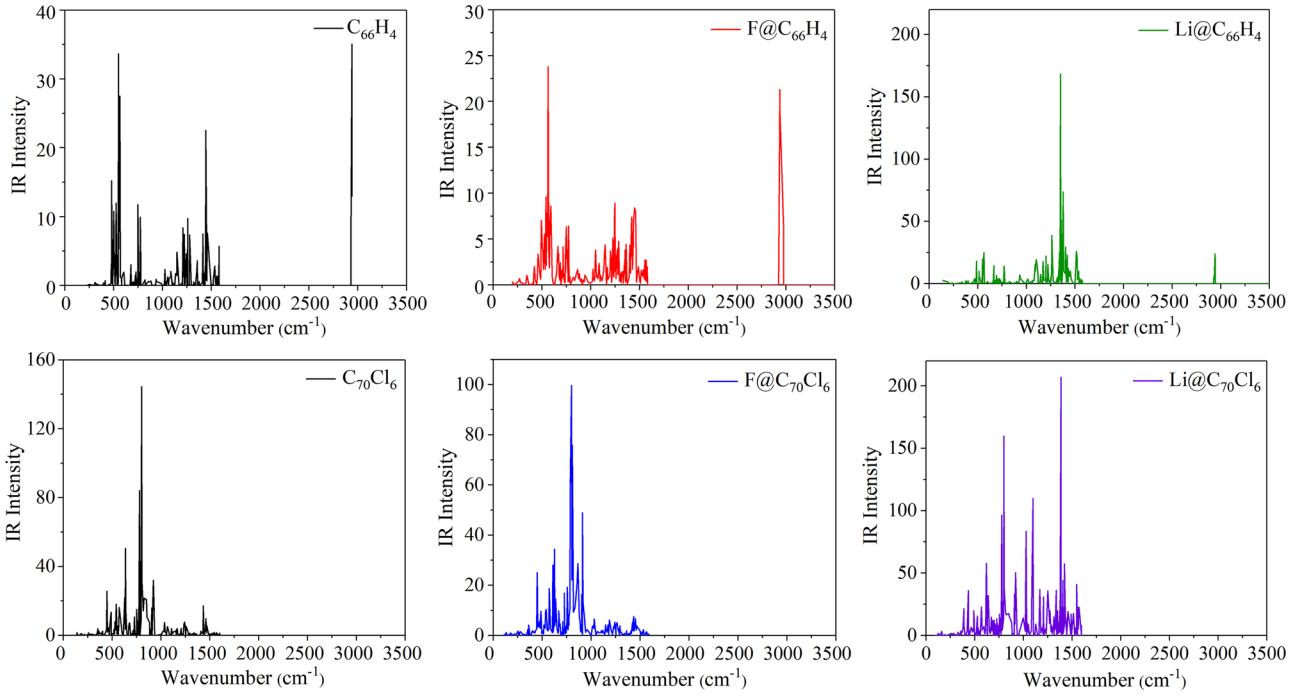

Figure 2. Simulated infrared spectra of $C_{66}H_4$, $C_{70}Cl_6$, $F@C_{66}H_4$, $F@C_{70}Cl_6$, $Li@C_{66}H_4$, and $Li@C_{70}Cl_6$.

Table 2. Dipole Moment (μ, Debye) and Static Polarizability (α, au) of $X@C_{66}H_4$ and $X@C_{70}Cl_6$ (X = F and Li), and Natural Population Analysis (NPA) Charges (e) of Encapsulated Atoms

molecules	μ	α	atom	charge
$F@C_{66}H_4$	4.24	631.00	F	−0.43
$Li@C_{66}H_4$	4.72	652.86	Li	+0.88
$F@C_{70}Cl_6$	3.32	772.86	F	−0.42
$Li@C_{70}Cl_6$	4.20	814.47	Li	+0.89
$C_{66}H_4$	4.38	621.98		
$C_{70}Cl_6$	3.48	770.45		

is poor in both HOMO and LUMO. Such charge distributions are induced by the electron transfer from the internal Li atoms to the carbon cage, forming a strong ionic interaction and a weak covalent interaction between them, which also leads to lower encapsulation energies. On the other hand, the LUMO of $F@C_{66}H_4$ and $F@C_{70}Cl_6$ is mainly contributed by the C atoms close to the F atom. According to our static polarizability calculations, the static polarizability of fullerene derivatives increases after encapsulating Li atoms and F atoms, providing evidence of the charge transfer between the encapsulated atoms and the carbon cage.

Thus, natural bond orbital (NBO) population analysis was performed to quantitatively investigate the electron transfer behavior of $X@C_{66}H_4$ and $X@C_{70}Cl_6$ (X = F and Li). As the first ionization energy of a Li atom is low and the electron affinity of a F atom is strong, the valence electron of the inner Li atom transfers to the carbon cage, and similarly, the external carbon cage transfers electrons to the F atom. Referring to the ground-state electronic configurations of Li and F ([Xe] $2s^1$ and [Xe] $2s^22p^5$), the number of transferred electrons is supposed to be one in both cases. Counterintuitively, NBO results in Table 2 show that charges on the Li and F atoms of $Li@C_{66}H_4$, $Li@C_{70}Cl_6$, $F@C_{66}H_4$, and $F@C_{70}Cl_6$ are +0.88 e, +0.89 e, −0.43 e, and −0.42 e, respectively, none of which

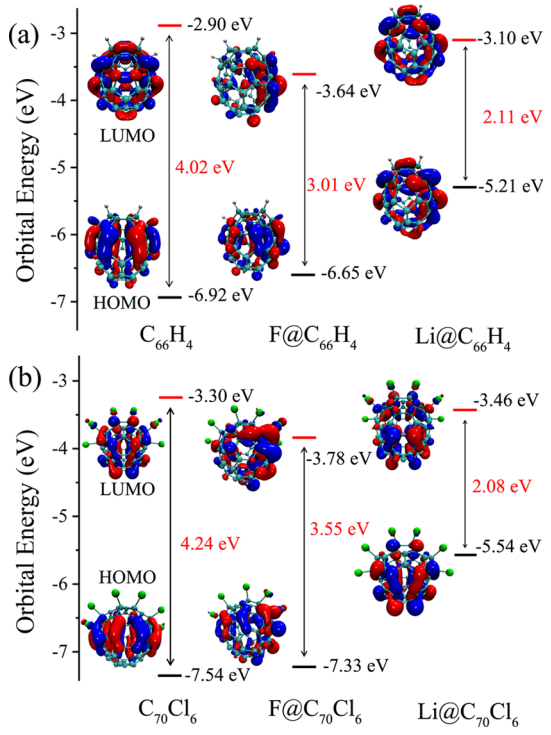

Figure 3. (a) HOMO and LUMO diagrams of $C_{66}H_4$, $F@C_{66}H_4$, and $Li@C_{66}H_4$. (b) HOMO and LUMO diagrams of $C_{70}Cl_6$, $F@C_{70}Cl_6$, and $Li@C_{70}Cl_6$. The values of the red lines, the black lines, and the red font represent the LUMO, HOMO, and HOMO−LUMO gap values, respectively. Cyan, white, green, pink, and mauve balls denote C, H, Cl, F, and Li atoms, respectively.

reaches 1 e. From theoretical perspective, this phenomenon is the consequence of the back-donation of the charge between the encapsulated atoms and the carbon cage. In other words, there is the back-donation of 0.12 e from the $C_{66}H_4$ cage to the Li atom in $Li@C_{66}H_4$, reducing the charge of the Li atom to

https://doi.org/10.1021/acsomega.1c02364
ACS Omega 2021, 6, 16234−16240

+0.88 *e*. In the same way, there is the back-donation of 0.57 electrons from the F atom to the $C_{66}H_4$ cage in F@$C_{66}H_4$, reducing the charge of the F atom to −0.43 *e*. It is then identified that the back-donation of charge between the F atom and the carbon cage is stronger. Now, that the electron transfer toward the carbon cage is less hindered, it can be inferred that $C_{66}H_4$ and $C_{70}Cl_6$ are better electron acceptors than electron donors.

Previous research studies have reported that the back-donation of charge indicates the covalent interactions between the inner atoms and the carbon cage.[35,36] Herein, we first performed localized orbital locator (LOL) analysis on X@$C_{66}H_4$ and X@$C_{70}Cl_6$ (X = F and Li) to study such interactions. As shown in Figure 4, the LOL function between

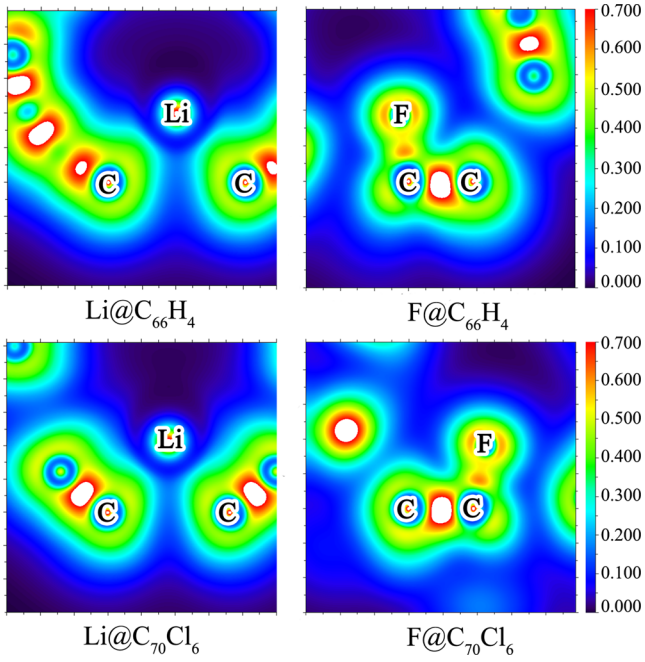

Figure 4. Localized orbital locator (LOL) map of F@$C_{66}H_4$, Li@$C_{66}H_4$, F@$C_{70}Cl_6$, and Li@$C_{70}Cl_6$. The plane is defined by the encapsulated atom and two carbon atoms.

Li atoms and carbon atoms is sparsely distributed, while a highly localized region occurs between F atoms and carbon atoms. This indicates that Li atoms and carbon atoms are mainly bound by electrostatic force and the covalent interaction is very weak, whereas F atoms interact strongly with carbon atoms through covalent bonds, consistent with the abovementioned NBO analysis. Focusing on the strong covalent interaction between F and C in F@$C_{66}H_4$ and F@$C_{70}Cl_6$, we further performed bond critical point (BCP) and Mayer bond order (MBO) calculations. The critical points of F@$C_{66}H_4$ and F@$C_{70}Cl_6$ are shown in Figure 5, where the BCPs between a F atom and carbon atoms are emphasized with a red circle mark. Typical bond descriptors of BCPs and the MBO results are given in Table 3. For both structures, the values of $\rho_{BCP} > 0$, $H_{BCP} < 0$, $|V_{BCP}|/G_{BCP} > 2$ and MBO > 0.8 can be observed, indicating the strong covalent interaction between the F atom and carbon atoms. Besides, the bond between F and C in F@$C_{70}Cl_6$ possesses larger values of ρ_{BCP}, $|V_{BCP}|/G_{BCP}$ and MBOs, thus proving that the covalent interaction between F and $C_{70}Cl_6$ is stronger than that between F and $C_{66}H_4$.

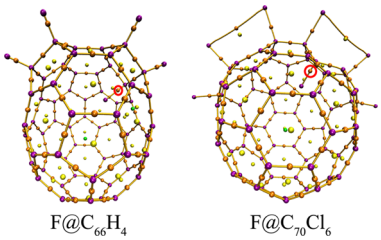

Figure 5. Critical points (CPs) of F@$C_{66}H_4$ and F@$C_{70}Cl_6$. Each purple, orange, yellow, and green ball represents a critical point of (3, −3), (3, −1), (3, +1), and (3, +3), respectively. BCPs between a F atom and carbon atoms are marked in red circles.

One of the benefits of the considerable charge transfer from the internal atoms is the improvement of the redox properties of $C_{66}H_4$ and $C_{70}Cl_6$. We then applied vertical ionization potential (VIP) and vertical electron affinity (VEA) of X@$C_{66}H_4$ and X@$C_{70}Cl_6$ (X = F and Li) to interpret such effects. Table 4 shows our calculation results. Compared with $C_{66}H_4$ and $C_{70}Cl_6$, the fullerenes encapsulating F and Li atoms exhibit lower VIP and higher VEA values so that they are not only easier to lose electrons but also easier to accept electrons. In a word, the presence of inner atoms improves the redox properties of $C_{66}H_4$ and $C_{70}Cl_6$. On the other hand, compared with Li@$C_{66}H_4$ and Li@$C_{70}Cl_6$, the fullerene derivatives encapsulating F atoms have higher VIP and VEA values, indicating that their reducibility and antioxygenic properties are better.

In application, fullerenes are famous for their good nonlinear optical properties due to the three-dimensional (3D) delocalized π-electron conjugated system. In recent years, it has been discovered that the presence of metal atoms can further improve the nonlinear optical properties of fullerenes.[37,38] As we introduced Li atoms to $C_{66}H_4$ and $C_{70}Cl_6$, the first hyperpolarizability (β) was calculated to reveal the influence of Li atoms on the nonlinear optical properties of $C_{66}H_4$ and $C_{70}Cl_6$. The hyperpolarizability β is defined as:

$$\beta = [(\beta_{xxx} + \beta_{xyy} + \beta_{xzz})^2 + (\beta_{yyy} + \beta_{yzz} + \beta_{yxx})^2 + (\beta_{zzz} + \beta_{zxx} + \beta_{zyy})^2]^{1/2} \quad (1)$$

where β_{ijk} is tensorial components of the first hyperpolarizability. The β values of $C_{66}H_4$ and $C_{70}Cl_6$ are 608.55 and 770.45 au, respectively. The encapsulation of Li atoms in $C_{66}H_4$ and $C_{70}Cl_6$ cages strongly impacts nonlinear optical responses of $C_{66}H_4$ and $C_{70}Cl_6$, resulting in a steep increase in the β values of Li@$C_{66}H_4$ and Li@$C_{70}Cl_6$, which are 7.90 times of original $C_{66}H_4$ and 10.19 times of original $C_{70}Cl_6$, which creates favorable conditions for their applications in advanced electronic devices. A Li atom significantly improves the nonlinear optical properties of fullerenes, which makes us suspect whether a F atom also has this ability. Therefore, we calculated the first hyperpolarizabilities of F@$C_{66}H_4$ and F@$C_{70}Cl_6$. The result is disappointing that the encapsulation of the F atom into $C_{66}H_4$ can marginally increase the first hyperpolarizability. Moreover, when the F atom is encapsulated into $C_{70}Cl_6$, the first hyperpolarizability decreases rather than increases. The comparison between the two results reflects that the halogen F atom is indeed inferior to the metal Li atom in improving the nonlinear optics of fullerenes. The reason why metal atoms can increase the first hyperpolarizability of fullerenes has been proposed as the reason

https://doi.org/10.1021/acsomega.1c02364
ACS Omega 2021, 6, 16234−16240

Table 3. Density of All Electrons (ρ_{BCP}), Energy Density (H_{BCP}), and Ratios of Potential Energy Density to Lagrangian Kinetic Energy ($|V_{BCP}|/G_{BCP}$) of BCPs in F@$C_{66}H_4$ and F@$C_{70}Cl_6$, and the Bond Length (d) and MBO Values between a F Atom and Carbon Atoms

molecules	bond	ρ_{BCP}	H_{BCP}	$\lvert V_{BCP}\rvert/G_{BCP}$	d	MBO
F@$C_{66}H_4$	C_{43}–F_{71}	0.191	−0.205	2.330	1.497	0.844
F@$C_{70}Cl_6$	C_{21}–F_{77}	0.199	−0.223	2.359	1.482	0.908

Table 4. Vertical Ionization Potential (VIP, eV), Vertical Electron Affinity (VEA, eV), and First Hyperpolarizability (β, au) of F@$C_{66}H_4$, Li@$C_{66}H_4$, F@$C_{70}Cl_6$, Li@$C_{70}Cl_6$, $C_{66}H_4$, and $C_{70}Cl_6$

molecule	VIP	VEA	β
F@$C_{66}H_4$	7.01	3.33	673.16
Li@$C_{66}H_4$	5.67	2.61	4810.42
F@$C_{70}Cl_6$	7.66	3.57	619.72
Li@$C_{70}Cl_6$	5.97	3.00	7848.96
$C_{66}H_4$	7.39	2.40	608.55
$C_{70}Cl_6$	7.98	2.78	770.45

for the electron transfer from the metal atom to the external carbon cage and the symmetry reduction after metal atom encapsulation.[39] The abovementioned NBO population analysis shows that the inner Li atoms transfer 0.88 and 0.89 electrons to the carbon cages of $C_{66}H_4$ and $C_{70}Cl_6$, respectively. Moreover, the symmetry of the parent cages of $C_{66}H_4$ and $C_{70}Cl_6$ are C_{2v} and C_s, respectively. The symmetry of Li@$C_{66}H_4$ is reduced to C_s and the symmetry of Li@$C_{70}Cl_6$ remains unchanged. Therefore, the phenomenon of improving the nonlinear optical properties with encapsulating Li atoms can be well explained.

CONCLUSIONS

In summary, we conducted a systematic study on the structures and electronic properties of X@$C_{66}H_4$ and X@$C_{70}Cl_6$ (X = F and Li) through density functional theory calculations. It was found that the encapsulation of F and Li atoms has a slight effect on the deformation of the total cage frame of $C_{66}H_4$ and $C_{70}Cl_6$, but the strong covalent interaction between a F atom and a carbon cage results in the collapse of the local C atoms in the cage. In addition, the encapsulation of F atoms in fullerene derivatives is easier. Frontier molecular orbitals analysis shows that the encapsulation of F and Li atoms leads to the reduction of the HOMO–LUMO gap, which is mainly due to the additional energy levels introduced by the encapsulated atoms. According to NBO results, compared with electron donors, $C_{66}H_4$ and $C_{70}Cl_6$ are better electron-acceptor materials. Moreover, there is a back-donation of charge between the inner atoms and the carbon cage, which indicates covalent interactions between the inner atoms and the carbon cage. Through the analyses of LOL, AIM, and MBO, we found that due to the weak back-donation of charge between a Li atom and a carbon cage, strong ionic and weak covalent interactions occur between the Li atom and the carbon cage, while a strong covalent interaction occurs between the F atom and the carbon cage. The presence of inner F and Li atoms improves the redox properties and polarizabilities of X@$C_{66}H_4$ and X@$C_{70}Cl_6$. We also found that the presence of Li atoms can significantly improve the nonlinear optical properties of $C_{66}H_4$ and $C_{70}Cl_6$, while halogen F atoms can only slightly increase or even decrease the first hyperpolarizability. The work in this paper may help to understand the different effects of F and Li atoms on the electronic properties of fullerenes and promote the potential applications of X@$C_{66}H_4$ and X@$C_{70}Cl_6$ in the field of nanoelectronics.

COMPUTATIONAL METHOD

The structural optimization, vibration frequency, and electronic structure calculations of $C_{66}H_4$, $C_{70}Cl_6$, F@$C_{66}H_4$, F@$C_{70}Cl_6$, Li@$C_{66}H_4$, and Li@$C_{70}Cl_6$ were performed using the hybrid density functional theory B3LYP exchange–correlation functional[40−42] with the def2-SVP basis set[43] as implemented in the Turbomole 7.4 package.[44] The Li and F atoms were encapsulated into the cavity of optimized $C_{66}H_4$ and $C_{70}Cl_6$. We designed encapsulation structures with different internal atom positions to screen out the most stable configurations, based on which frequency calculations were conducted to remove the metastable configurations. The electronic structures of $C_{66}H_4$, $C_{70}Cl_6$, F@$C_{66}H_4$, F@$C_{70}Cl_6$, Li@$C_{66}H_4$, and Li@$C_{70}Cl_6$ were calculated with finer precision on the M06-2X[45]-D3[46]/def2-TZVP[43] basis set. Subsequently, the dipole moment and polarizability were calculated with B3LYP/ma-def2-SVP[47,48] and the first hyperpolarizability was calculated with BHandHLYP[49]/ma-def2-SVP. The interactions between inner atoms and external carbon cages were studied via the Mayer bond order (MBO) analysis,[50] localized orbital locator (LOL) analysis,[51] and atoms in molecules (AIM)[52] theory analysis in Multiwfn 3.8.[53] Meanwhile, infrared spectra of Li@$C_{66}H_4$, F@$C_{66}H_4$, Li@$C_{70}Cl_6$, and F@$C_{70}Cl_6$ were simulated with B3LYP/def2-SVP. Due to the systematical errors and the use of resonance approximation, we corrected the frequency with the correction factor of 0.9671.[54] To explore the difficulty level of the encapsulating atom into a carbon cage, the encapsulation energies (E_{en}) of endohedral fullerene derivatives, X@$C_{66}H_4$ and X@$C_{70}Cl_6$, were calculated using the following equations with the basis set superposition error (BSSE) corrections considered:

$$E_{en} = E(C_{66}H_4) + E(X) - E(X@C_{66}H_4) \quad (2)$$

$$E_{en} = E(C_{70}Cl_6) + E(X) - E(X@C_{70}Cl_6) \quad (3)$$

where E(X@$C_{66}H_4$), E(X@$C_{70}Cl_6$), E($C_{66}H_4$), E($C_{70}Cl_6$), and E(X) are the electronic energies correspondingly. The atom X represents a Li atom and a F atom, respectively.

AUTHOR INFORMATION

Corresponding Authors

Baisheng Sa − *Key Laboratory of Eco-materials Advanced Technology, College of Materials Science and Engineering, Fuzhou University, Fuzhou 350108, P. R. China;* orcid.org/0000-0002-9455-7795; Email: bssa@fzu.edu.cn

Tao Yu − *State Key Laboratory of Fluorine & Nitrogen Chemicals, Xi'an Modern Chemistry Research Institute, Xi'an 710065, P. R. China; School of Chemistry and Chemical Engineering, Southeast University, Nanjing 211189, P. R. China;* Email: fischer@wo.cn

https://doi.org/10.1021/acsomega.1c02364
ACS Omega 2021, 6, 16234−16240

Authors

Ying Zhang − *Key Laboratory of Eco-materials Advanced Technology, College of Materials Science and Engineering, Fuzhou University, Fuzhou 350108, P. R. China*

Zhao Zheng − *Key Laboratory of Eco-materials Advanced Technology, College of Materials Science and Engineering, Fuzhou University, Fuzhou 350108, P. R. China*

Yitao Si − *International Research Center for Renewable Energy, State Key Laboratory of Multiphase Flow, Xi'an Jiaotong University, Xi'an 710049, P. R. China; State Key Laboratory of Fluorine & Nitrogen Chemicals, Xi'an Modern Chemistry Research Institute, Xi'an 710065, P. R. China*

Hengyi Li − *Fujian Applied Technology Engineering Center of Power Battery Materials, Fujian College of Water Conservancy and Electric Power, Yongan, Fujian 366000, China*

Cuilian Wen − *Key Laboratory of Eco-materials Advanced Technology, College of Materials Science and Engineering, Fuzhou University, Fuzhou 350108, P. R. China;* orcid.org/0000-0002-0410-606X

Bo Wu − *Key Laboratory of Eco-materials Advanced Technology, College of Materials Science and Engineering, Fuzhou University, Fuzhou 350108, P. R. China;* orcid.org/0000-0002-7676-2736

Complete contact information is available at: https://pubs.acs.org/10.1021/acsomega.1c02364

Notes

The authors declare no competing financial interest.

■ ACKNOWLEDGMENTS

This work was supported by the National Key Research and Development Program of China (No. 2017YFB0701701), the National Natural Science Foundation of China (Nos. 21973012 and 21978311), the Natural Science Foundation of Fujian Province (Nos. 2020J01351 and 2020J01474), the Scientific Research Project of Jinjiang Science and Education Park of Fuzhou University (Nos. 2019-JJFDKY-01 and 2019-JJFDKY-02), and the 'Qishan Scholar" Scientific Research Startup Project of Fuzhou University.

■ REFERENCES

(1) Kroto, H. W.; Heath, J. R.; O'Brien, S. C.; Curl, R. F.; Smalley, R. E. C_{60}: Buckminsterfullerene. *Nature* **1985**, *318*, 162−163.

(2) Chai, Y.; Liu, X.; Wu, B.; Liu, L.; Wang, Z.; Weng, Y.; Wang, C. In Situ Switching of Photoinduced Electron Transfer Direction by Regulating the Redox State in Fullerene-Based Dyads. *J. Am. Chem. Soc.* **2020**, *142*, 4411−4418.

(3) Chandler, H. J.; Stefanou, M.; Campbell, E. E. B.; Schaub, R. Li@C_{60} as a Multi-State Molecular Switch. *Nat. Commun.* **2019**, *10*, No. 2283.

(4) Hashikawa, Y.; Fushino, T.; Murata, Y. Double-Holed Fullerenes. *J. Am. Chem. Soc.* **2020**, *142*, 20572−20576.

(5) Miklitz, M.; Turcani, L.; Greenaway, R. L.; Jelfs, K. E. Computational Discovery of Molecular C_{60} Encapsulants with an Evolutionary Algorithm. *Commun. Chem.* **2020**, *3*, No. 10.

(6) Zhang, K.; Wang, C.; Zhang, M.; Bai, Z.; Xie, F.-F.; Tan, Y.-Z.; Guo, Y.; Hu, K.-J.; Cao, L.; Zhang, S.; Tu, X.; Pan, D.; Kang, L.; Chen, J.; Wu, P.; Wang, X.; Wang, J.; Liu, J.; Song, Y.; Wang, G.; Song, F.; Ji, W.; Xie, S.-Y.; Shi, S.-F.; Reed, M. A.; Wang, B. A Gd@C_{82} Single-Molecule Electret. *Nat. Nanotechnol.* **2020**, *15*, 1019−1024.

(7) Zhang, L.; Wang, C.; Bao, J.; Kalkan, A. K. Single-Photon Oxidation of C_{60} by Self-Sensitized Singlet Oxygen. *Commun. Chem.* **2020**, *3*, No. 71.

(8) Karton, A.; Waite, S. L.; Page, A. J. Performance of DFT for C_{60} Isomerization Energies: A Noticeable Exception to Jacob's Ladder. *J. Phys. Chem. A* **2019**, *123*, 257−266.

(9) Popov, A. A.; Yang, S.; Dunsch, L. Endohedral Fullerenes. *Chem. Rev.* **2013**, *113*, 5989−6113.

(10) Chai, Y.; Guo, T.; Jin, C.; Haufler, R. E.; Chibante, L. P. F.; Fure, J.; Wang, L.; Alford, J. M.; Smalley, R. E. Fullerenes with Metals Inside. *J. Phys. Chem. A* **1991**, *95*, 7564−7568.

(11) Stevenson, S.; Rice, G.; Glass, T.; Harich, K.; Cromer, F.; Jordan, M. R.; Craft, J.; Hadju, E.; Bible, R.; Olmstead, M. M.; Maitra, K.; Fisher, A. J.; Balch, A. L.; Dorn, H. C. Small-Bandgap Endohedral Metallofullerenes in High Yield and Purity. *Nature* **1999**, *401*, 55−57.

(12) Morinaka, Y.; Sato, S.; Wakamiya, A.; Nikawa, H.; Mizorogi, N.; Tanabe, F.; Murata, M.; Komatsu, K.; Furukawa, K.; Kato, T.; Nagase, S.; Akasaka, T.; Murata, Y. X-ray Observation of a Helium Atom and Placing a Nitrogen Atom Inside He@C_{60} and He@C_{70}. *Nat. Commun.* **2013**, *4*, No. 1554.

(13) Zhao, J.; Du, Q.; Zhou, S.; Kumar, V. Endohedrally Doped Cage Clusters. *Chem. Rev.* **2020**, *120*, 9021−9163.

(14) Yu, Y.; Slanina, Z.; Wang, F.; Yang, Y.; Lian, Y.; Uhlik, F.; Xin, B.; Feng, L. $Ho_2O@D_3(85)$-C_{92}: Highly Stretched Cluster Dictated by a Giant Cage and Unexplored Isomerization. *Inorg. Chem.* **2020**, *59*, 11020−11027.

(15) Yu, P.; Shen, W.; Bao, L.; Pan, C.; Slanina, Z.; Lu, X. Trapping an Unprecedented Ti_3C_3 Unit Inside the Icosahedral C_{80} Fullerene: A Crystallographic Survey. *Chem. Sci.* **2019**, *10*, 10925−10930.

(16) Zhao, J.; Huang, X.; Jin, P.; Chen, Z. Magnetic Properties of Atomic Clusters and Endohedral Metallofullerenes. *Coord. Chem. Rev.* **2015**, *289*−*290*, 315−340.

(17) Li, J.; Zhao, F.; Wang, T.; Nie, M.; Li, J.; Wei, Z.; Jiang, L.; Wang, C. Ethylenediamine Functionalized Fullerene Nanoparticles as Independent Electron Transport Layers for High-Efficiency Inverted Polymer Solar Cells. *J. Mater. Chem. A* **2017**, *5*, 947−951.

(18) Lapin, N. A.; Krzykawska-Serda, M.; Dilliard, S.; Mackeyev, Y.; Serda, M.; Wilson, L. J.; Curley, S. A.; Corr, S. J. The Effects of Non-Invasive Radiofrequency Electric Field Hyperthermia on Biotransport and Biodistribution of Fluorescent [60]Fullerene Derivative in a Murine Orthotopic Model of Breast Adenocarcinoma. *J. Controlled Release* **2017**, *260*, 92−99.

(19) Zhou, Y.; Deng, R.; Zhen, M.; Li, J.; Guan, M.; Jia, W.; Li, X.; Zhang, Y.; Yu, T.; Zou, T.; Lu, Z.; Guo, J.; Sun, L.; Shu, C.; Wang, C. Amino Acid Functionalized Gadofullerene Nanoparticles with Superior Antitumor Activity via Destruction of Tumor Vasculature in Vivo. *Biomaterials* **2017**, *133*, 107−118.

(20) Chen, X.; Ge, F.; Lai, N. Probing the Catalytic Activity and Poisoning-Tolerance Ability of Endohedral Metallofullerene $Fe_n@C_{60}$ (n = 1−7) Catalysts in the Oxygen Reduction Reaction. *J. Electrochem. Soc.* **2020**, *167*, No. 024515.

(21) Yaghobi, M.; Koohi, A. Nonlinear Optical and Structural Properties of M@C_N Endohedrals (M = Li, Ca and Sc, N = 60 and 70). *Mol. Phys.* **2010**, *108*, 119−126.

(22) Wang, L.; Ye, J.-T.; Wang, H.-Q.; Xie, H.-M.; Qiu, Y.-Q. Third-Order Nonlinear Optical Properties of Endohedral Fullerene $(H_2)_2$@C_{70} and $(H_2O)_2@C_{70}$ Accompanied by the Prospective of Novel $(HF)_2@C_{70}$. *J. Phys. Chem. C* **2018**, *122*, 6835−6845.

(23) Kroto, H. W. The Stability of the Fullerenes C_n, with n = 24, 28, 32, 36, 50, 60 and 70. *Nature* **1987**, *329*, 529−531.

(24) Yang, S.; Ioffe, I. N.; Troyanov, S. I. Chlorination-Promoted Skeletal Transformations of Fullerenes. *Acc. Chem. Res.* **2019**, *52*, 1783−1792.

(25) Mazaleva, O. N.; Ioffe, I. N.; Jin, F.; Yang, S.; Kemnitz, E.; Troyanov, S. I. Experimental and Theoretical Approach to Variable Chlorination-Promoted Skeletal Transformations in Fullerenes: The Case of C_{102}. *Inorg. Chem.* **2018**, *57*, 4222−4225.

(26) Zhong, Y.-Y.; Chen, Z.-C.; Du, P.; Cui, C.-H.; Tian, H.-R.; Shi, X.-M.; Deng, S.-L.; Gao, F.; Zhang, Q.; Cong-Li, G.; Zhang, X.; Xie,

S.-Y.; Huang, R.-B.; Zheng, L.-S. Double Negatively Curved C_{70} Growth through a Heptagon-Involving Pathway. *Angew. Chem., Int. Ed.* **2019**, *58*, 14095−14099.
(27) Tian, H.-R.; Chen, M.-M.; Wang, K.; Chen, Z.-C.; Fu, C.-Y.; Zhang, Q.; Li, S.-H.; Deng, S.-L.; Yao, Y.-R.; Xie, S.-Y.; Huang, R.-B.; Zheng, L.-S. An Unconventional Hydrofullerene $C_{66}H_4$ with Symmetric Heptagons Retrieved in Low-Pressure Combustion. *J. Am. Chem. Soc.* **2019**, *141*, 6651−6657.
(28) Srivastava, A. K.; Pandey, S.; Pandey, A.; Misra, N. C_{60} as Electron Acceptor and Donor: A Comparative DFT Study of Li@C_{60} and F@C_{60}. *Aust. J. Chem.* **2018**, *71*, 953−956.
(29) Pavanello, M.; Jalbout, A. F.; Trzaskowski, B.; Adamowicz, L. Fullerene as an Electron Buffer: Charge Transfer in Li@C_{60}. *Chem. Phys. Lett.* **2007**, *442*, 339−343.
(30) Sadlej-Sosnowska, N.; Mazurek, A. P. Electron Density Distribution in Endohedral Complexes of Fullerene C_{60}, Calculated Based on the Gauss Law. *J. Chem. Inf. Model.* **2012**, *52*, 1193−1198.
(31) Salehzadeh, S.; Yaghoobi, F.; Bayat, M. Theoretical Studies on the Interaction of Some Endohedral Fullerenes {$[X@C_{60}]^-$ (X=F^-, Cl^-, Br^-) or $[M@C_{60}]$ (M=Li, Na, K)} with $[Al(H_2O)_6]^{3+}$ and $[Mg(H_2O)_6]^{2+}$ Cations. *Comput. Theor. Chem.* **2014**, *1034*, 73−79.
(32) Cui, C.-X.; Zhang, Z.-P.; Zhu, L.; Qu, L.-B.; Zhang, Y.-P.; Lan, Y. Reactivity and Regioselectivity in Diels−Alder Reactions of Anion Encapsulated Fullerenes. *Phys. Chem. Chem. Phys.* **2017**, *19*, 30393−30401.
(33) Rodríguez-Fortea, A.; Balch, A. L.; Poblet, J. M. Endohedral Metallofullerenes: A Unique Host-Guest Association. *Chem. Soc. Rev.* **2011**, *40*, 3551−3563.
(34) Popov, A. A.; Dunsch, L. Structure, Stability, and Cluster-Cage Interactions in Nitride Clusterfullerenes $M_3N@C_{2n}$ (M = Sc, Y; 2n = 68−98): A Density Functional Theory Study. *J. Am. Chem. Soc.* **2007**, *129*, 11835−11849.
(35) Bao, L.; Peng, P.; Lu, X. Bonding inside and outside Fullerene Cages. *Acc. Chem. Res.* **2018**, *51*, 810−815.
(36) Yang, S.; Wei, T.; Jin, F. When Metal Clusters Meet Carbon Cages: Endohedral Clusterfullerenes. *Chem. Soc. Rev.* **2017**, *46*, 5005−5058.
(37) Abedi, M.; Shamlouei, H. R. Structure, Electrical and Nonlinear Optical Properties of M@C_{20} (M = Li, Na, K, Be, Mg and Ca) Nanoclusters. *Bull. Mater. Sci.* **2018**, *41*, No. 137.
(38) Gao, F.-W.; Zhong, R.-L.; Sun, S.-L.; Xu, H.-L.; Zhao, L.; Su, Z.-M. Charge Transfer and First Hyperpolarizability: Cage-Like Radicals $C_{59}X$ and Lithium Encapsulated Li@$C_{59}X$ (X=B, N). *J. Mol. Model.* **2015**, *21*, No. 258.
(39) Rostampour, E. Effect of Coulomb Interaction on the Second-Order Nonlinear Optical and Magneto-Optical Properties of the Endohedral La@C_{82} Crystal with Spatial Dispersion. *Optik* **2019**, *198*, No. 162955.
(40) Lee, C.; Yang, W.; Parr, R. G. Development of the Colle-Salvetti Correlation-Energy Formula into a Functional of the Electron Density. *Phys. Rev. B* **1988**, *37*, 785−789.
(41) Becke, A. D. Density-Functional Thermochemistry. III. The Role of Exact Exchange. *J. Chem. Phys.* **1993**, *98*, 5648−5652.
(42) Stephens, P. J.; Devlin, F. J.; Chabalowski, C. F.; Frisch, M. J. *Ab Initio* Calculation of Vibrational Absorption and Circular Dichroism Spectra Using Density Functional Force Fields. *J. Phys. Chem. A* **1994**, *98*, 11623−11627.
(43) Weigend, F.; Ahlrichs, R. Balanced Basis Sets of Split Valence, Triple Zeta Valence and Quadruple Zeta Valence Quality for H to Rn: Design and Assessment of Accuracy. *Phys. Chem. Chem. Phys.* **2005**, *7*, 3297−3305.
(44) *TURBOMOLE V7.4 2019. A Development of University of Karlsruhe and Forschungszentrum Karlsruhe GmbH, 1989-2007, TURBOMOLE GmbH, since 2007*. http://www.turbomole.com (last accessed May 28, 2021).
(45) Zhao, Y.; Truhlar, D. G. The M06 Suite of Density Functionals for Main Group Thermochemistry, Thermochemical Kinetics, Noncovalent Interactions, Excited States, and Transition Elements: Two New Functionals and Systematic Testing of Four M06 Functionals and 12 Other Functionals. *Theor. Chem. Acc.* **2008**, *120*, 215−241.
(46) Grimme, S.; Antony, J.; Ehrlich, S.; Krieg, H. A Consistent and Accurate ab initio Parametrization of Density Functional Dispersion Correction (DFT-D) for the 94 Elements H-P_u. *J. Chem. Phys.* **2010**, *132*, No. 154104.
(47) Zheng, J.; Xu, X.; Truhlar, D. G. Minimally Augmented Karlsruhe Basis Sets. *Theor. Chem. Acc.* **2011**, *128*, 295−305.
(48) Pritchard, B. P.; Altarawy, D.; Didier, B.; Gibson, T. D.; Windus, T. L. New Basis Set Exchange: An Open, Up-to-Date Resource for the Molecular Sciences Community. *J. Chem. Inf. Model.* **2019**, *59*, 4814−4820.
(49) Becke, A. D. A new mixing of Hartree−Fock and local density-functional theories. *J. Chem. Phys.* **1993**, *98*, 1372−1377.
(50) Mayer, I. Bond Orders and Valences From ab initio Wave Functions. *Int. J. Quantum Chem.* **1986**, *29*, 477−483.
(51) Schmider, H. L.; Becke, A. D. Chemical Content of the Kinetic Energy Density. *J. Mol. Struct.: THEOCHEM* **2000**, *527*, 51−61.
(52) Bader, R. F. W. Atoms in Molecules. *Acc. Chem. Res.* **1985**, *18*, 9−15.
(53) Lu, T.; Chen, F. Multiwfn: A Multifunctional Wavefunction Analyzer. *J. Comput. Chem.* **2012**, *33*, 580−592.
(54) Kesharwani, M. K.; Brauer, B.; Martin, J. M. L. Frequency and Zero-Point Vibrational Energy Scale Factors for Double-Hybrid Density Functionals (and Other Selected Methods): Can Anharmonic Force Fields Be Avoided? *J. Phys. Chem. A* **2015**, *119*, 1701−1714.

https://doi.org/10.1021/acsomega.1c02364
ACS Omega 2021, 6, 16234−16240